Patricia Morillas Varela

TOWARDS A BIOSENSOR FOR THE DETECTION OF ACUTE LYMPHOBLASTIC LEUKEMIA

Final Degree Project

Supervised by

Dra. Beatriz Prieto Simón

Co-supervised by

Deepanshu Verma

Degree in Biomedical Engineering

UNIVERSITAT ROVIRA I VIRGILI

Tarragona

2021-2022

INDEX

1 Introduction

1.1 Objectives

In Acute Lymphoblastic Leukemia (ALL), the term "lymphocyte" refers to the fact that this disease originates from immature lymphocytes, a type of white blood cell that constantly and excessively reproduces, thus affecting two types of lymphocytes (B cells and T cells); whereas "acute" represents that the disease can progress very rapidly, in fact, if left untreated, it can cause premature death [1].

ALL starts in the bone marrow (if 20% of the bone marrow consists of cancerous lymphocytes, the disease is considered leukemia), where hematopoietic cells are formed. In this pathology malignant cells are produced. The uncontrolled proliferation of these cells with abnormal differentiation and long-lasting life, determines a high number of circulating blasts in the blood, the replacement of healthy cells by malignant ones and, sometimes, the spread to other parts of the body, such as the liver, spleen, central nervous system, lymph nodes and testicles (in men). Symptoms of these events usually include fatigue, pallor, infection, bone pain, easy bruising and bleeding.

This cancer is the most common cancer in pediatrics with 75-80% among all acute leukemias. The incidence of this disease peaks in children between 2 and 5 years of age. On the other hand, 25% of tumors in children under 15 years of age and 19% of cysts in patients under 19 years of age are based on ALL. The sex most affected by this disease is male, especially at puberty.

As it evolves in an accelerated and aggravating manner, this disease must be diagnosed early, thus achieving an early treatment to favour the prognosis in pediatric patients, since most of those who receive treatment are cured.

The treatment of childhood acute lymphoblastic leukemia consists of three phases [2]:

- **Remission induction:** the goal is to achieve remission of the disease by destroying the leukemic cells in the blood and bone marrow.

- **Consolidation and intensification:** once leukemia is remitting, the aim is to destroy the remaining leukemic cells in the body to prevent relapse.

- **Maintenance:** the goal is the same as in the consolidation and intensification phase but administering lower doses. Failure to take the drugs prescribed by the physician in maintenance therapy is more likely to result in relapse.

Four standard treatments are used to destroy the cells [2]:

- **Chemotherapy:** drugs are used to stop cancer cells from forming and/or destroy them. This chemotherapy can be systemic (oral), intrathecal (injected into the cerebrospinal fluid), regional (affects only one area) or combined (more than one drug is used).

- **Radiation therapy:** high-energy x-rays or other radiation are used to destroy cancer cells or prevent them from multiplying.

- **Chemotherapy with stem cell transplantation:** immature blood cells taken from a donor are transplanted into the patient after chemotherapy. These stem cells will then grow into the body's blood cells and restore the destroyed ones.

- **Targeted therapy:** therapy that is less damaging to normal cells than those mentioned above. It uses drugs or other substances that identify and attack the targeted cancer cells. Therapy with tyrosine kinase inhibitors (TKIs), monoclonal antibodies and proteasome inhibitors is often implemented.

In some ALL patients, the above treatments can only achieve long-term remission. This means that in the symptom-free patient, no cells belonging to the disease are found when tested. In other patients, it is not sufficient to control the disease because the disease is more aggressive. In this case, a bone marrow transplant at an early stage of the disease may help to achieve long-term remission [3].

A bone marrow transplant begins with chemotherapy, with or without radiation, to destroy the diseased cells and bone marrow, preparing the body to receive treatment. The transplant replaces the diseased blood-forming cells with healthy cells. Usually, this transplant is performed allogeneically because there is less risk that the disease may return. In these types of transplants, healthy blood-forming cells from a family member, donor or umbilical blood unit are used. The replacement cells are infused into the patient's bloodstream where they reach the bone marrow, where they begin to make healthy red blood cells, white blood cells and platelets. The whole process can last from weeks to months [3].

Despite all the treatments discussed, ALL represents the most common type of childhood malignancy and, despite significant progress in current treatment, 20-30% of affected children relapse and the causes are still uncertain [4].

Early diagnosis through the detection of key biomarkers at the point of testing for this disease in children is of utmost importance to avoid relapses. The early detection of the disease at an early stage is considered of utmost importance to make rapid treatment decisions, thus favouring, with more probabilities, the cure of the patient. Therefore, this project aims to gain insight into the development of a biosensor capable of sensitively detecting key biomarkers in the diagnosis of ALL. Biosensors are analytical devices capable of providing such information. Among the various types of biosensors, those based on electrochemical transduction have the potential to provide a rapid, highly reliable, sensitive and accurate quantitative response at low cost and with the ease of miniaturization. These biosensors must be designed according to the requirements of the application, so it is essential to design the transducer and select the best bioreceptors depending on the characteristics of the biomarker and the "type of sample (e.g. blood, serum, plasma, etc) where they are located.

Up to now, only one electrochemical sensor has been reported for the detection of ALL. It combined a DNA sensor and an aptasensor to detect the presence of BCR-ABL1, a mutant gene, and carcinoembryonic antigen (CEA), a cancer biomarker. A positive test result of the DNA sensor meant that a person had a mutant gene and was at the risk of a cancer. A positive test result of the aptasensor meant that the person already had the disease. Sensitivity, selectivity, and reproducibility of the biosensors were evaluated [14].

Many studies highlighted the role of microRNAs (miRNA), small (17-25 nucleotides) single-stranded non-coding RNAs that modify gene expression by sequence targeting through translational repression, as cancer biomarkers. miRNAs play a very important role in the regulation of normal haematopoiesis and their alteration could contribute to leukemogenesis, moreover, analysis of their expression helps to understand the development of phenotypes and biological functions of miRNAs in childhood ALL [5].

One such study, demonstrated that miR-128, miR-146a, miR-155, miR-181a and miR-195 can not only be used as biomarkers in ALL diagnosis but also, disease monitoring [5].

Among all those miRNAs, miR-181a showed its key role in the development and differentiation of T and B lymphocytes. Moreover, it repressed the expression of genes that play a role in thymocyte maturation (such as Bcl-2, CD69 and T-cell receptor). In addition, the miR-181 family was found to be significantly overexpressed in leukemia [5]. Future studies should focus on miR-181 both as therapeutic target and biomarker for diagnosis. For that reason, **miR-181a** was chosen as biomarker in this work. Free miRNAs are present in blood at very low concentrations, so highly sensitive tools are required for their detection. This is

why the final aim of the project will be the detection of exosomal miRNAs. Exosomal miRNAs have recently been highlighted as powerful biomarkers, due to the advantages of being protected by the exosome lipid bilayer, and present at higher concentrations in the exosomal contents. Here, we aim to explore the potential of various porous structures to enable the detection of exosomes and exosomal miRNA previously identified as biomarkers of ALL. However, as a first step, this works focuses on developing the sensing part devoted to the detection of miRNA, which will be combined in future works with the capture and quantification of exosomes. Such novel biosensor with sequential detection of specific exosomes and a target miRNA is expected to facilitate accurate detection of ALL at the early stages of the disease.

In this project a sensing platform based on a porous material was needed. The two main requirements of this biosensor are the high sensitivity needed to detect very low concentrations of miRNA, and a platform which is capable in dealing complex biological samples. Thus, the reason to use a porous material to build the sensing platform is justified by mainly three reasons: first, the large surface area to volume ratio allows to achieve higher sensitivity owing to larger active area, second, the possibility to use a sensing mechanism based on pore blockage that has been demonstrated to improve the sensitivity compared to using a flat surface, and third, the possibility to exploit the morphological features to minimise interferences based on size exclusion effects. Semiconducting porous materials will be fabricated, and their chemical functionalization will be addressed to function as a sensing platform. Finally, the most suitable detection mechanism for electrochemical detection of the target analyte (exosomal miRNAs) will be designed and optimized.

1.2 Fabrication of porous alumina membranes for biosensing applications

Among porous materials able to provide the advantages described in the previous section, Porous Anodic Aluminium Oxide (pAAO) was selected as the choice of platform due to the following properties: quasi-periodic arrangement of the nanopore channels, narrow distribution of pore sizes and interpore distances, relative ease to control the porous scales and self-ordering qualities by anodization conditions, excellent thermal stability, and very low cost.

First, some chemical characteristics of pAAO should be understood. Thermodynamically, certain metals or semi-metals such as aluminium, under ambient conditions react with oxygen to form a thin layer of metal oxide. The oxide film formed on the metal surface usually has a thickness of 2-3 nm. This reaction [6] can be explained by the following chemical equation (1):

$$2Al(s) + \frac{3}{2}O_2(g) \rightarrow Al_2O_3(s) \qquad \Delta G° = -1582\ KJ \cdot mol^{-1} \qquad (1)$$

Electrochemically, the process of anodizing aluminium to make pAAO is carried out by partially immersing the anode and cathode in electrolytes such as aqueous solutions of phosphoric acid, oxalic acid, or sulfuric acid. An anodizing voltage is applied between cathode (Pt) and anode (aluminium), pores nucleate and begin to grow on the surface of the Al (Figure 1a-d). This growth is due to competition between oxidation and dissolution. First, aluminium oxide grows at the aluminium-alumina interface due to the counter migration of Al^{3+} and O^{2-} through the oxide barrier layer. Second, aluminium oxide (Al_2O_3) dissolves at the interface between alumina and electrolyte [6].

At the same time as these reactions occur, other reactions take place. Since the electrical conductivity of aluminium oxide is very low, ionic transport (Je) predominates for the main ionic species (Al^{3+} and O^{2-}) across the alumina-alumina interface. During the first seconds of the anodization process, the current density decreases sharply. As a result, the aluminium substrate is covered by a thin, compact layer of Al_2O_3, typically 2-3 nm. Then, the current

density reaches its minimum value and increases to its maximum. At this time, pores nucleate in the oxide layer and the current density decreases slightly to a constant value at which pore growth is maintained and is directly related to the time of anodization [6].

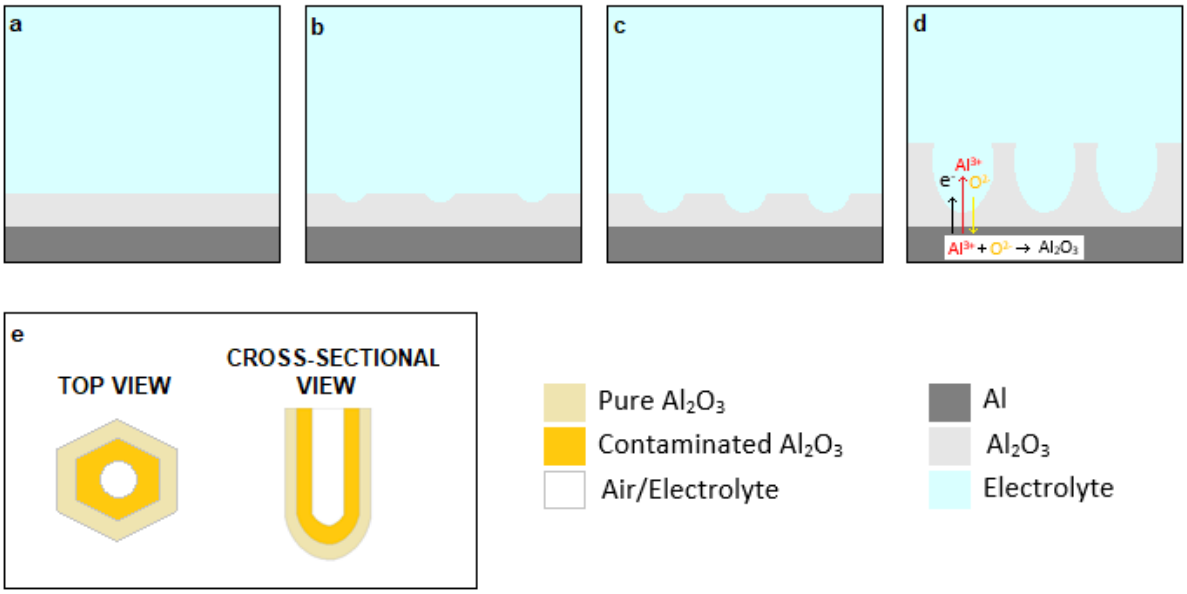

Figure 1. Growth process of porous alumina through different stages: a) initial state of the aluminium substrate, b) dissolution of the oxide, c) formation of pores, d) pore growth, e) structure and chemical composition of a nanoporous alumina pore.

The aim of the fabrication process is the following:

Figure 2. Effect on the aluminium at each step of the fabrication process. It starts with bare aluminium and continues with pore growth until it finally has open pores.

From a chemical point of view, two main regions can be distinguished in the structure of a NAA pore (Figure 1e). The first is an inner layer composed basically of pure alumina. The second is a layer that is contaminated by anionic species of the acid electrolyte. The ratio of the thickness of the inner layer to the thickness of the outer layer depends on the acid electrolyte for NAAs fabricated under disordered or ordered pore growth regimes. An important property of these layers is that the outer layer is less resistant to chemical etching than the inner layer, which prevents the structure from collapsing even at high porosity [6].

NAA is fabricated by simple electrochemical anodization of aluminium and consists of closely packed hexagonal arrays of nanopores from top to bottom obtained during anodization.

The simple electrochemical approach uses a two-step anodization procedure for the fabrication of highly ordered nanostructures based on the self-ordering phenomenon (Figure 2). As depicted in Table 1, geometrical and structural characteristics as pore density (PD), porosity (P), inter-pore distance (dIP), pore diameter (dp), pore growth rate (Rp) and barrier layer thickness (τ) that can be controlled by anodization parameters such as pH, temperature (T), time (t), voltage (V), potential, concentration, and the type of acid electrolyte used [6-7].

Parameters	PD	P	dIP	dP	Rp	τ
pH	D	D	D	D	I	D
T	D	D	-	D	D	I
t	D	D	-	D	I	-
V		-	D	D	D	D
Potential	D	D	D	D	-	-
Concentration	-	-	I	D	-	-
Type: oxalic acid (250-500 V)	-	-	60-70 nm	80-200 nm	-	-

Table 1. Relation between anodizing parameters and structural characteristics of nanoporous. *D* and *I* is used to declare a *directly proportional* and an *indirectly proportional, respectively.*

By changing the various fabrication parameters, pore size and thickness of the pAAO substrate can be tuned to match the sensing requirements.

For biosensing purposes, pAAO membranes are placed on top of an electrode, to enable a sensing mechanism based on measuring the pore blockage caused upon analyte recognition by the bioreceptor immobilised on the pAAO membrane.

2 Material and methods

The aim was to develop a sensor for DNA sensing, as a first step towards the design of a miRNA sensor, and for our study the substrate used for this purpose was pAAO.

The process to develop the biosensor was as follows:

1. Fabrication of pAAO membranes
2. Appropriate surface functionalisation
3. DNA conjugation
4. Activation of carbon screen printed electrodes
5. Electrochemical measurements
6. Substrate characterization

In the section further details about each of these steps are discussed.

2.1 Fabrication of porous alumina

The aluminium was purchased from Goodfellow Cambridge Limited with 99.999 % of purity.

The sheet of aluminium was cut into squares of 2 cm x 2 cm using a flatbed paper cutter tool. As aluminium is extremely malleable, it was pressed between two copper plates to make sure it is flat on the macro-scale before proceeding with further steps.

2.1.1 Cleaning and electropolishing

To achieve a homogeneous pAAO layer, commercial aluminium substrates were pre-treated prior to anodization. The pure aluminium squares (2x2 cm^2) used as substrates were cleaned with acetone (purchased from ITW reagents, Spain), deionized water, and ethanol 96 % v/v (C_2H_5OH) (purchased from ITW reagents, Spain) to remove all impurities and residual

grease. Next, a copper plate which acts as the connection of anodes was sanded to remove any oxide layer on it. It was then washed with ethanol and dried again with compressed air.

Once this was done, the aluminium substrates were placed onto a custom-made PVC cell, with holes (4-7) to expose aluminium to the acid electrolyte. The PVC cell and the copper plate were screwed together with aluminium samples clamped in between them.

It is vital to make sure that the cell does not have any leaks and hence the PVC cell was filled with water and left for 2-3 minutes to ensure it did not lose liquid during further fabrication steps. After ensuring a proper fit of the cell, the electropolishing electrolyte was added in the PVC well. The electrolyte used for electropolishing was a 4:1 v/v acid solution of ethanol (C_2H_5OH) and perchloric acid ($HClO_4$). Perchloric acid (70 %) reagent grade was purchased from Scharlau. Electropolishing was carried out under constant stirring. The direction of stirring was alternated between clockwise and counterclockwise every minute using a switch (Figure 3). A voltage was applied between the cathode (Pt wire) and the anode (copper plate) and the aluminium was oxidized but no oxide was formed due to the chemical conditions of the electrolyte used. The electropolishing process was carried out by applying 20 V for 6 minutes at 5 ºC under a constant stirring rate of 300 rpm to remove the bubbles generated on the Al Surface. When the process finished a graph of the next characteristics was achieved (Figure 4).

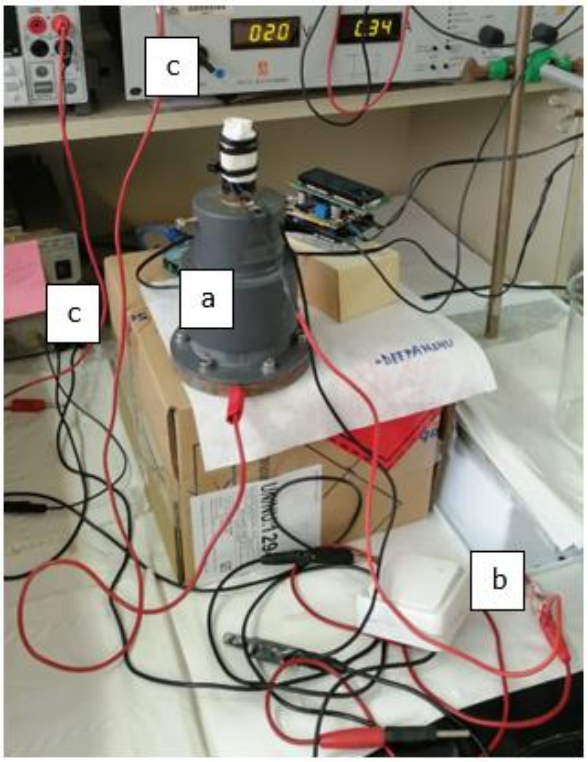

Figure 3. Assembly of the electrochemical polishing process: a) PVC cell, b) switch, and c) power sources.

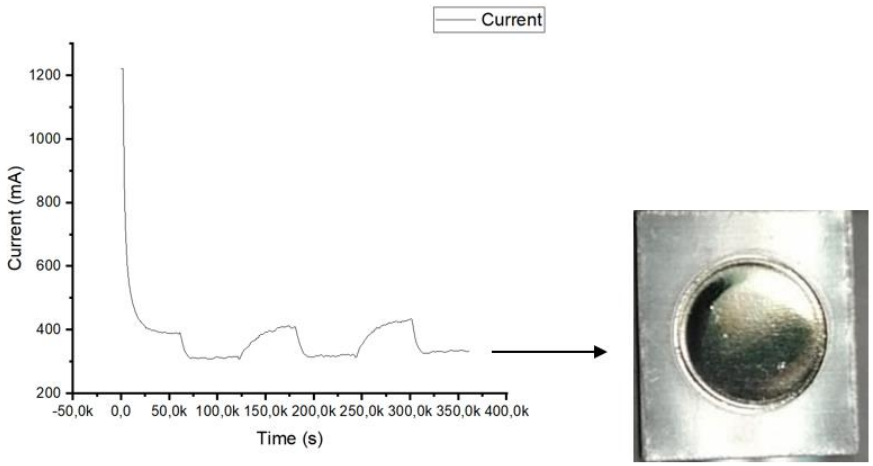

Figure 4. Current versus time profile for electropolishing at a constant potential of 20V.

2.1.2 First anodization

After electropolishing, the complete cell was cleaned with ethanol and water and dried with compressed air. It is extremely important to make sure there are no traces of electropolishing electrolyte as that may change the geometrical properties of pAAO.

As different electrolytes can be used to achieve different pore sizes: Oxalic acid (30-35 nm), sulfuric acid (15-20 nm) and phosphoric (90-100 nm). The choice of electrolyte for anodization was 0.3 M oxalic acid (98 %) (purchased from Sigma Aldrich) ($H_2C_2O_4$) since a pore size between 30-50 nm was needed. Again, similar to setting up the PVC cell in the previous step, the well in the PVC cell was filled with oxalic acid exposing the electropolished aluminium surface to the acid. The anodization was carried out typically between 0-5 ºC. The temperature of the electrolyte was measured by introducing a thermometer in the PVC cell (Figure 5). After the temperature of the cell was stable for 30 minutes the anodization was started at 40 V for a period of 20 hours under constant stirring. The anodization was controlled using a custom-coded LabVIEW program which automatically run and ended the program after the desired parameters (Figure 6) were achieved.

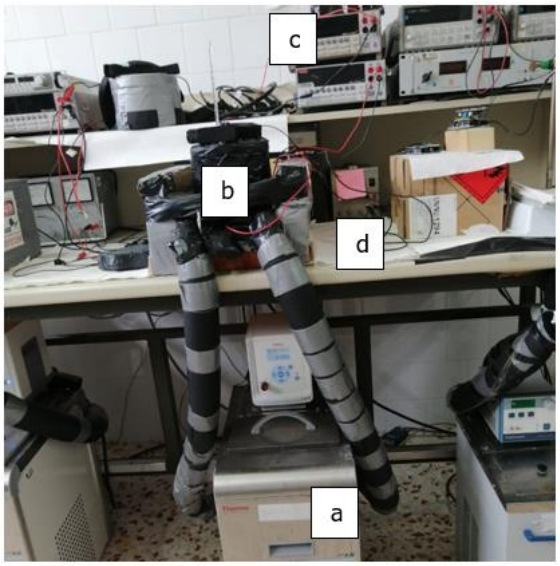

Figure 5. Assembly of the first anodization process: a) cooler, and b) PVC cell on top of the cooler and protected to maintain the temperature controlled by a thermometer, c) multimeter, and d) power source.

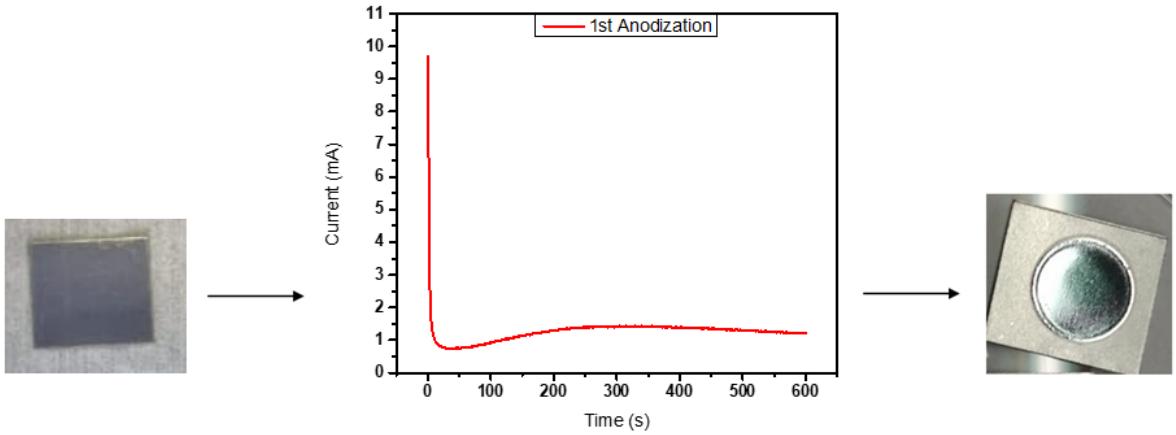

Figure 6. Current versus time profile during first anodization at a constant anodization potential of 40V.

2.1.3 Removal of unordered pores

After the first anodization a chemical etching step was performed in which the objective was to remove the first layer of alumina. To achieve this, first the PVC cell was unscrewed, and the samples were cleaned with deionized water and ethanol (C_2H_5OH) and dried with compressed air.

The unordered pores that were formed during first anodization were etched via chemical etching route. The alumina substrates were immersed in an acid solution of H_3PO_4 and H_2CrO_4 (1.8-6% wt). The phosphoric acid (≤85 %) and chromic acid (≤98 %) were purchased from Sigma Aldrich.

The etching process was carried out in a beaker placed on a hot plate at 70 ºC under constant stirring of 450 rpm for 1 hour (Figure 7). The samples were then washed with water and dried with compressed air.

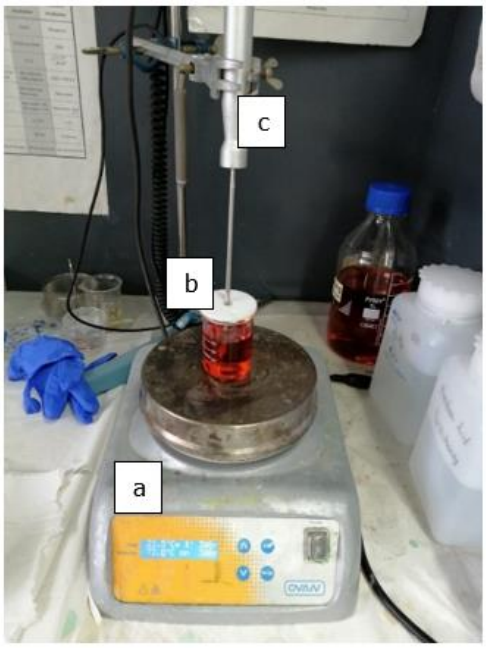

Figure 7. The assembly for removal of unordered pores: a) hot plate, b) beaker where alumina substrates were immersed in the acid solution, and c) thermometer.

2.1.4 Second anodization

After the first anodization, many irregular hexagonal pores were obtained on the surface, therefore, to obtain ordered concavities with better pore regularity and without imperfections a chemical etching was done to remove unordered pAAO. After the removal of unordered pores from the aluminium substrate, the sites from which the pores nucleated provided us with an aluminium substrate with concavities where the pores could grow during the second anodization. Hence, the anodization this time yielded a better pore regularity.

The aluminium substrates were clamped between the PVC cell and the copper plate similar to the first anodization. It is to be noted that the first and second anodizations were carried out at the same anodization voltage. However, the thickness of the porous membrane was controlled by controlling the total charge accumulated during the anodization process. A charge of 4 C was needed to grow a pAAO film of 1 µm on a sample area of 1.76 cm^2.

Again, the anodization was controlled using a custom-coded LabVIEW program which automatically run and ended the program after the desired parameters (Figure 8) were achieved.

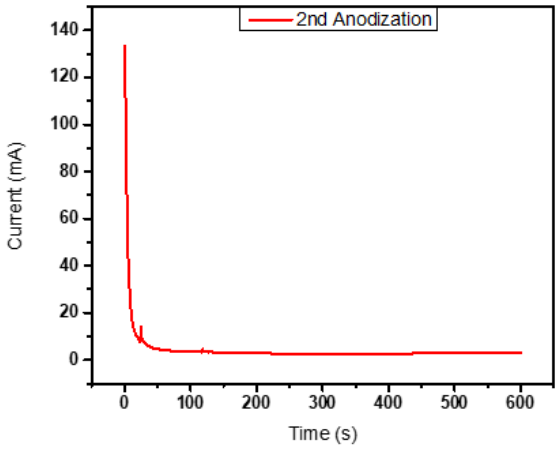

Figure 8. Current versus time profile during second anodization at a constant anodization potential of 40V.

2.1.5 Chemical etching of aluminium and barrier oxide layer removal

The so formed porous film on top of aluminium cannot be used for electrochemical biosensing applications. For our specific use of a pAAO substrate on top of an electrode in an electrochemical cell, a pAAO film with a through hole morphology is desired. Which means that a pAAO membrane with ordered pores on top and bottom of the membrane is needed.

For this purpose, first etching of the aluminium substrate below the Paao film was performed.

The substrates were clamped in a teflon cell faced down so that the side of the substrate with aluminium was exposed. The aluminium was exposed to a saturated acid solution of $CuCl_2$ and HCl (22.6 mg/mL of $CuCl_2$ in 12.6 wt % $HCl{\cdot}2H_2O$) ($CuCl_2$ ≤ 99 % and HCl (37 %) were purchased from Sigma Aldrich and Scharlau, respectively). After approximately 15 minutes the aluminium was etched exposing the barrier oxide layer below the pAAO film (Figure 9).

Further, to remove the barrier oxide layer with the objective to achieve a free-standing nano pAAO membrane the barrier oxide layer was exposed to an acid treatment in 5 % phosphoric acid solution at 55 °C in a muffle furnace for a time of 23 minutes. This acid treatment opened

the barrier oxide layer with pores of 20-25 nm. Further pore widening treatment in the same acid for 10 minutes provided us with pores of a diameter of ~45 nm.

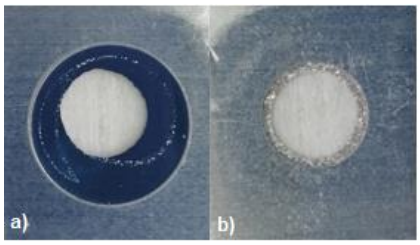

Figure 9. a) Front side of the aluminium, and b) back side of the aluminium etched.

2.2 Surface modification

Commercial and fabricated pAAO membranes were modified following the steps depicted in Figure 10.

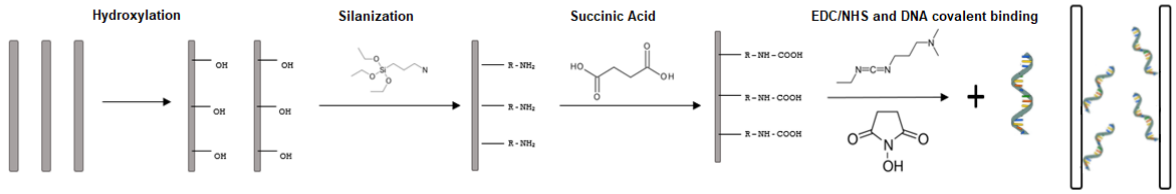

Figure 10. Step-wise modification of pAAO membranes.

2.2.1 Hydroxylation

To introduce OH groups on the pAAO's surface hydroxylation was performed. First, the pAAO substrates were cleaned with water and ethanol. An oil bath was preheated at 180 ºC and the hydrogen peroxide (purchased from Alfa Aesar) temperature maintained at 100 ºC (Figure 11). The substrates were treated in 30% aqueous H_2O_2 at 160 ºC (oil bath temperature) for 1 hour. Then the pAAO was removed and transferred directly to an oven at 60 ºC for a period of 2 hours.

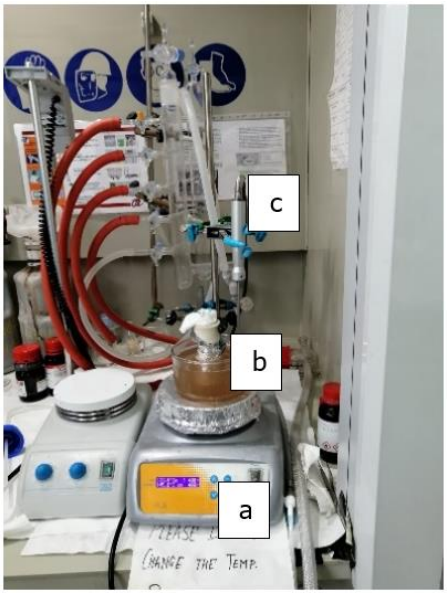

Figure 11. Assembly of the hydroxylation process: a) hot plate, b) substrates inside flat bottom glass vessel treated with H_2O_2 inside an oil bath, and c) thermometer.

2.2.2 Silanization

The pAAO substrates were dried and transferred to a teflon holder in a round bottom tube and sealed with rubber stopper, then 99.85 % extra-dry toluene (purchased from Sigma Aldrich) was introduced in the tube with a syringe under constant nitrogen flow (Figure 12). The reaction temperature was maintained at 28 ºC. Silanization was done via wet-chemical route in a moisture-free environment using (3-aminopropyl)triethoxysilane (APTES) (purchased from Sigma Aldrich) in dry toluene (5% v/v) for 30 minutes. The substrate was taken out and rinsed in toluene (purchased from Alfa Aesar) and dried with nitrogen. Following which, membranes were dried in the oven for 1 hour at 100 ºC. The membranes were then stored in vacuum until further use.

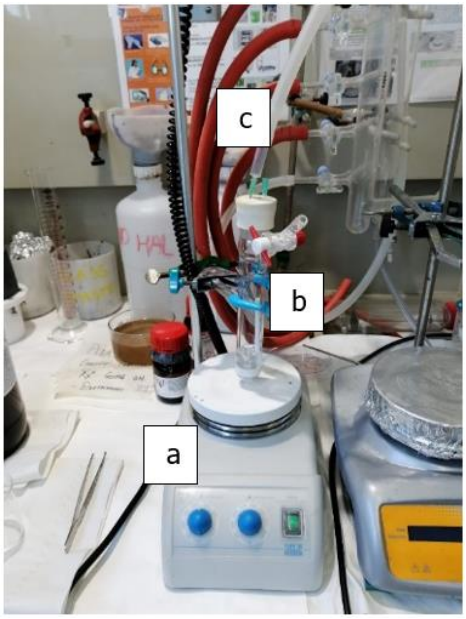

Figure 12. Assembly of the silanization process: a) hot plate, b) round bottom tube with samples inside, and c) nitrogen flow.

2.2.3 Succinic acid

After silanization, 0.2 M of succinic acid (purchased from Sigma Aldrich) was added to 9.4 mL DMSO (purchased from Sigma Aldrich) and shaken well to mix. Then 0.1 M at pH 9.4 of $NaHCO_3$ was added to the solution. The silanized pAAO substrate was kept in a petri dish and the solution was poured on top. The reaction was allowed to proceed on a shaker for 30 minutes in dark. Finally, the substrates were washed with DMSO followed by water and dried with nitrogen.

2.2.4 EDC/NHS

Solutions of 10 mg/mL N-(3-dimethylaminopropyl)-N'-ethylcarbodiimide hydrochloride (EDC) and 15 mg/mL of N-hydroxysuccinimide (NHS) were prepared separately in 0.1 M 2-(N-morpholino)ethanesulfonic acid (MES) buffer, pH 5.4, and then mixed 1:1 (v/v). EDC and NHS were purchased from Sigma Aldrich.

Then 300 µL of this solution were deposited on each sample, and the samples were kept on the shaker for 30 minutes.

2.2.5 Incubation with DNA capture probe

The membranes were incubated with 100 µL of a 0.5 µM solution of ssDNA capture probe (5'-NH_2-C_6-GTCCACGCCGTAAACGATGTCGACTTGG-3') prepared in 0.1 M phosphate buffered saline (PBS) for sensors, and the same volume of 0.5 µM solution of a random ssDNA sequence (5'-5-NH_2-C_6-AGTTATCCCAGTCTTATAGGTAGGT-3') prepared in 0.1 M PBS for controls for a period of 1 hour at room temperature on a shaker followed by overnight incubation at 4 ºC.

2.2.6 Ethanolamine

Each sensor was incubated with 300 µL of 0.1 M ethanolamine (purchased from Sigma Aldrich) prepared in 0.1 M PBS at pH 7.4 during 1 hour at room temperature on the shaker.

2.3 Electrochemical techniques

The electrochemical measurements were done using a custom-built 3-electrode electrochemical teflon cell. The electrochemical cell comprised of a pAAO-modified carbon screen-printed electrode as working electrode, a Pt counter electrode, and a Ag/AgCl reference electrode.

Initially, stability measurements were done to ensure a stable baseline signal form the sensor and control electrodes. For stability measurements, up to 5 cycles of cyclic voltammetry, electrochemical impedance spectroscopy and square wave voltammetry were recorded with incubation of approximately 30 minutes between each measurement. The electrochemical measurements were performed with the electrolyte solution (730 µL) of 2 mM $K_4[Fe(CN)_6]$ and 2 mM $K_3[Fe(CN)_6]$ in 0.1 M PBS. The sensors were considered stable when at least 2 consecutive measurements were similar to each other.

After the platform was stable, the sensor cells and control cells were washed thouroughly and incubated with different concentrations (0.1 pM, 10 pM, 1 nM, 100 nM and 1 µM) of the target DNA for 30 minutes each. After incubation with each concentration, cyclic voltammetry, electrochemical impedance spectroscopy and square wave voltammetry were performed.

For electrode activation, characterisation of surface modification, and sensing, the following electrochemical techniques were used:

2.3.1 Cyclic voltammetry

Cyclic Voltammetry (CV) is a powerful tool to investigate the reduction and oxidation processes of molecular species. It is an electrochemical technique where the working electrode potential is ramped linearly versus time. After the set potential is reached the working electrode's potential is ramped in the opposite direction to return to the initial potential. These cycles of ramps in potential may be repeated as many times as needed (Figure 13). The current at the working electrode is plotted versus the applied voltage to give the cyclic voltammogram trace that is used to study electrochemical properties of an analyte [8].

When understanding a cyclic voltammogram, the x axis represents a parameter that is imposed on the system (that is applied potential (E)). While the y axis is the response, the resulting current (I). The two peaks (Iox and Ired) show the peak oxidation current and peak reduction current at oxidation potential (Eox) and reduction potential (Ered), respectively. The difference between the two peaks is called peak-to-peak separation (ΔEp).

The conditions used for CV were E start = -0.5 V, 0.8 V to -0.5 V, E step = 5 mV, 3 cycles, 1mA of current range and scan rate = 100 mV/s.

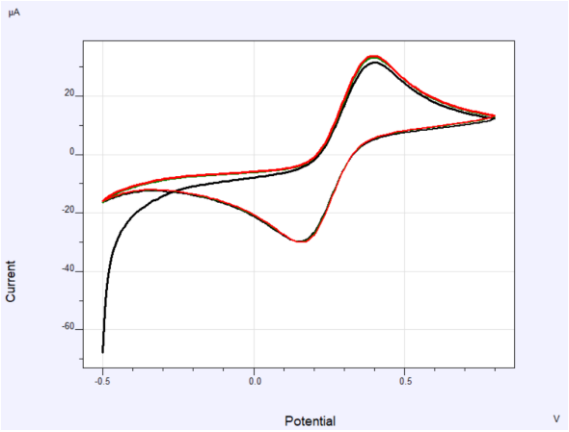

Figure 13. Example of a CV graph.

2.3.2 Electrochemical impedance spectroscopy

Electrochemical Impedance Spectroscopy (EIS) is a powerful technique that allows the study of capacitive, inductive and diffusion processes taking place in the electrochemical cell (Figure 14). It uses a small amplitude alternating current (AC) signal to probe the impedance characteristics of a cell. The name impedance "spectroscopy" is derived from the fact that the impedance is determined at different frequencies rather than a single frequency. Thus, an impedance spectrum is obtained that allows characterization of surfaces, layers or membranes, being sensitive to surface phenomena and changes in bulk properties, as well as exchange processes and diffusion processes [9].

The conditions used for EIS were E start = 0.2 V, 51 frequencies and 100 µA of current range.

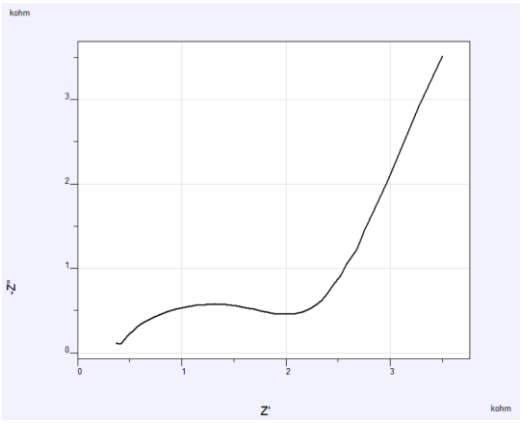

Figure 14. Example of an EIS spectrum.

2.3.3 Square wave voltammetry

Square Wave Voltammetry (SWV) is a very sensitive small amplitude electrochemical technique that was developed to isolate the faradaic signal contribution and the contribution of eddy currents. It is based on the principle that the signal-to-noise ratio increases with the square root of the sweep speed. The SWV time depends on the frequency, so as the frequency increases, the time constant decreases and the measured faradaic current increases, giving sharper and more defined peaks to the voltammogram [11-12].

In this voltammetry, a symmetrical square wave pulse is superimposed on a staircase wave giving rise to the square wave (Figure 15). The pulse duration, τ, is equal to the staircase length, and the superposition is obtained so that the forward pulse of the square wave

coincides with the first half of the staircase. Two other important parameters are Esw, the height of the square wave pulse, and Esc, the staircase rise for each step.

In square wave voltammetry, the current signal is the result of a difference between experimentally measured currents. The first current is measured at the end of the forward square wave pulse, and the second is measured at the end of the return square wave pulse; the difference results in a higher peak because the two individual signals are of opposite sign [13].

The conditions used for SWV were E start = -0.2 V, E ends = 0.8 V, E step = 5 mV, 1 cycle, 100 µA of current range, SQRWV frequency = 5 Hz and 25 mV of pulse amplitude.

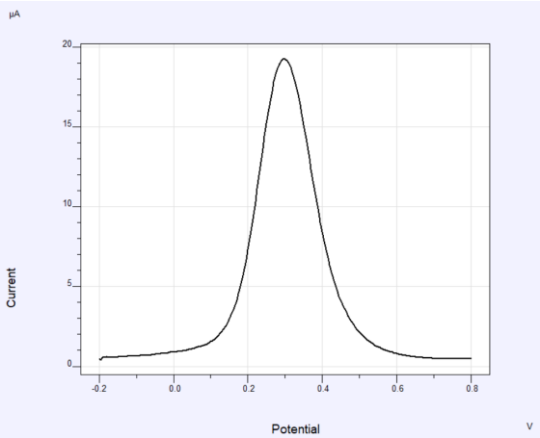

Figure 15. Example of a differential pulse voltammogram.

2.3.4 Activation of carbon screen printed electrodes (C-SPE)

C-SPE were purchased from Quasense. The as purchased electrodes require activation prior to their use to show a reproducible electrochemical response.

The C-SPE were activated by performing amperometry in 0.05 M carbonate buffer (pH 9.6) for 45 seconds at 1.2 V. After each amperometry cycle, Cyclic Voltammetry (CV) in 2 mM ferrocyanide and 2 mM ferricyanide solution prepared in PBS at pH 7.4 was performed. Before activation and after each cycle of activation, the third cyclic voltammogram for each step were recorded (Figure 16). The activation cycles were repeated till cyclic voltammograms corresponding to two consecutive activation steps were similar.

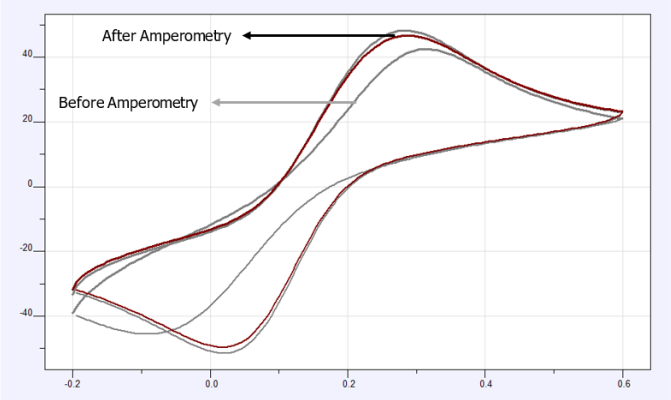

Figure 16. CV results before and after amperometry.

2.4 Characterization of porous alumina membranes

2.4.1 SEM

The Scanning Electron Microscope (SEM) is one of the most versatile instruments available that can provide information mainly about the surface topography and chemical composition.

For this reason, SEM was used as a characterization technique to check the pore size and thickness of the membranes. In this way, was known if the manufacturing and functionalization processes generated the expected results, otherwise, changes in these protocols were required.

2.4.2 FTIR

Infrared spectroscopy is a vibrational spectroscopy that deals with the IR spectrum providing information about functional groups.

IR spectrum plots IR absorbance or transmittance on the y axis vs scanning wavelength on the x axis. The molecules of the sample absorb at specific frequencies depending upon their oscillating frequencies and hence this frequency is the characteristic frequency of their structure. Basically, the frequency of the absorbed radiation matches the transition energy of the bond or group that vibrates.

The FTIR used for characterizing our porous membranes at each step of modification is an *FTIR spectrometer/Jasco 600 system* (Figure 17). The system in use is equipped to collect spectral data over MIR region. The system was used at every step of the functionalization process to ensure successful ssDNA binding. As the technique is qualitative in nature, it was used to analyse the groups introduced onto the membrane surface at each step.

Reflectance spectroscopy and a liquid nitrogen cooled MCT detector was used to capture the spectra. All spectra were collected as an average of 64 scans, with a resolution of 4 cm^{-1}, over the range of 450-4000 cm^{-1}. A background of air was used to correct the raw spectra.

Figure 17. Image of Jasco FTIR 6300 [17].

3 Results and discussion

3.1 Characterization results

In addition to commercial pAAO membranes, fabricated pAAO membranes were also used for our experiments, and thus the morphological characterization of the latter, was performed, via SEM to verify the pore size diameter before measurements. These membranes were later functionalized, followed by covalent immobilization of DNA capture probe prior to the electrochemical measurements. At each step of surface modification, these membranes were characterized using IR spectroscopy.

3.1.1 SEM analysis

The first sensing experiments were performed using 20 nm pore size commercial pAAO membranes purchased from Whatman. The SEM images in Figure 18 show these membranes feature an average pore size of 20 nm ± 6 nm and 188 nm ± 5 nm for front and back side, respectively. These membranes had a thickness of 60 µm. It is clearly visible that though these membranes were supposed to feature 20 nm pores the average pore size on both sides of the membrane was different.

The membranes as seen from the naked eye had a shiny and a matte side. The shiny side had the pore size as mentioned (20 nm) but the matte side had pore size much larger than the mentioned pore size.

The matte side was placed in direct contact to the C-SPE, leaving the shiny side exposed to the solution, as the shiny side had more uniform pores with much desirable pore size.

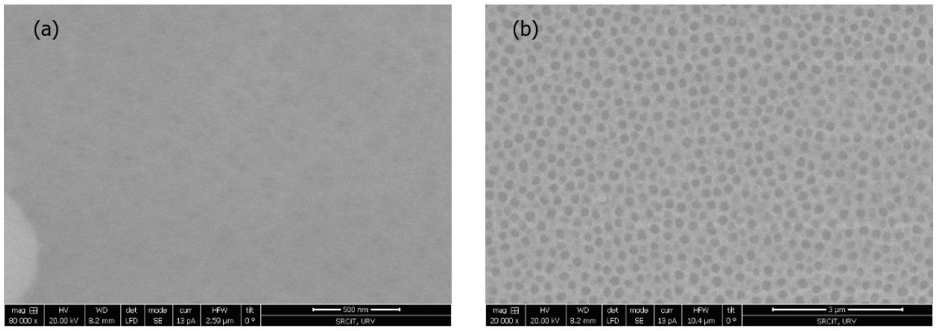

Figure 18. SEM images of a) front side, and b) back side of 20 nm pores commercial pAAO membranes.

The second sensing experiments were performed using fabricated membranes with pore size of 40 nm ± 5 nm and 50 nm ± 5 nm for front and back side, respectively (Figure 19). The fabrication conditions are the ones discussed in Material and methods sections of this thesis.

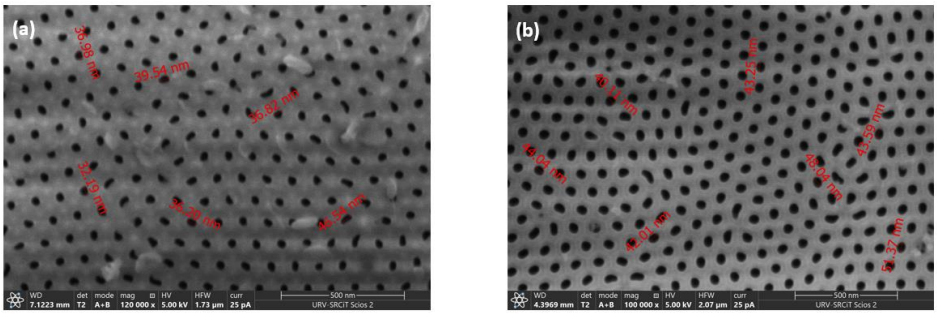

Figure 19. SEM images of pAAO membranes fabricated with 0.3 M oxalic acid at 40 V at 1°C a) front side pore size of approximately 40 nm, and b) back side pore size of approximately 45 nm.

3.1.2 IR Spectra

Infrared spectroscopy was used as a qualitative technique to identify the functional groups stepwise introduced on the pAAO substrate.

Further, IR was recorded at each step of membrane modification. IR at each step confirmed the presence of the expected functional groups. These include:

- **Hydroxylation**

  To allow silanization, OH groups are required on the pAAO surface, so hydroxylation with hydrogen peroxide is performed to introduce first those functional groups. Figure 20 shows the reflectance spectrum of this step which features a broad band at ~3400 cm^{-1} corresponding to the OH stretch.

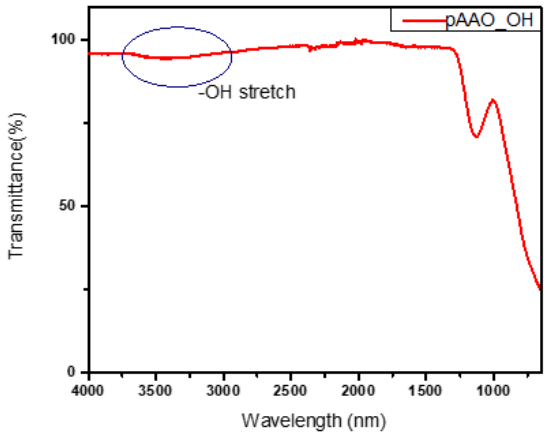

Figure 20. Reflectance spectrum of hydroxilated pAAO substrate shows the OH stretch at ~3400 cm^{-1}.

- **Silanization**

  Silanization was done with 5% (v/v) ratio of APTES in extra dry toluene under N_2 atmostphere for 30 minutes. A characteristic double peak at 2854 cm^{-1} and 2916 cm-1 was observed (Figure 21), which corresponds to the presence of C-H stretching from the methoxy groups.

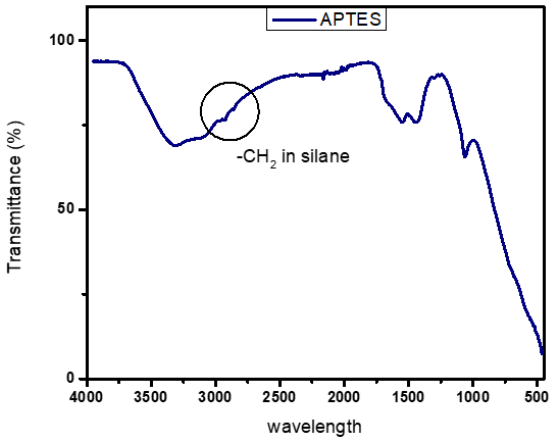

Figure 21. Reflectance spectrum of a silanized pAAO substrate.

- **Succinic acid treatment**

The silanized membranes were incubated with 0.2 M succinic acid in a solution of DMSO and 0.1 M at pH 9.4 of sodium bicarbonate to introduce carboxyl groups in the porous structure. New peaks at 1631 cm^{-1} and 1457 cm^{-1} were observed (Figure 22) corresponding to the amide bond and carboxyl group, respectively.

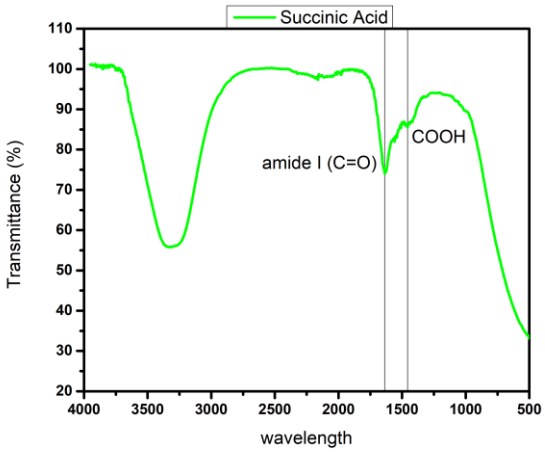

Figure 22. Reflectance spectrum of a silanized pAAO substrate upon reaction with succinic acid.

- **EDC/NHS activation and immobilization of ssDNA capture probe**

EDC reacted with the carboxylic acid and formed o-acylisourea, a highly reactive chemical that reacted with NHS and formed an NHS ester, which quickly reacted with the amine terminated ssDNA probe. Figure 23 compares the FTIR spectrum recorded after DNA conjugation to those previously taken after each functionalization step.

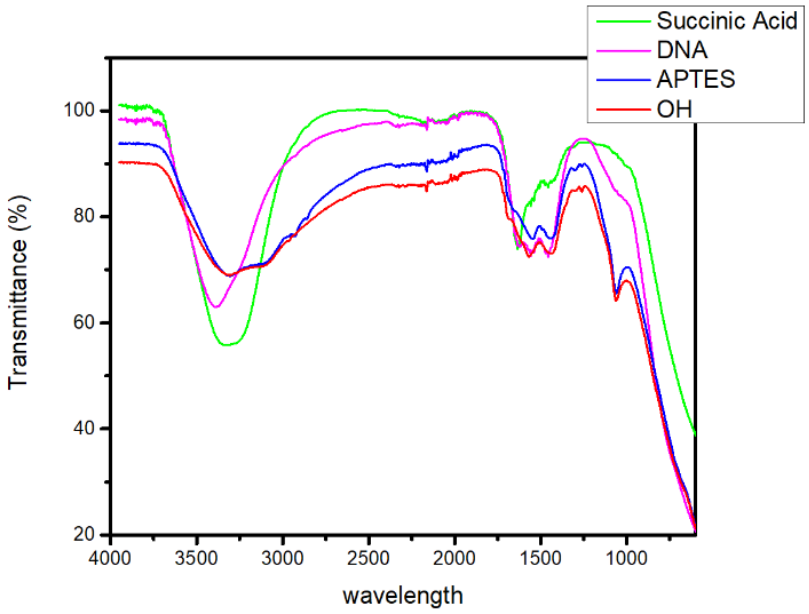

Figure 23. Reflectance spectrum comparing hydroxylated pAAO substrate (red), silanized pAAO substrate (blue), silanized pAAO substrate treated with succinic acid (green) and pAAO substrate after being activated with EDC/NHS and incubated with DNA capture probe (pink).

3.2 Sensing results

Working with porous substrates to build the sensing platform allows harnessing the measurement of the partial pore blockage caused upon analyte recognition as sensing mechanism. Upon DNA hybridization, pores undergo a partial blockage that can be electrochemically measured when adding a redox species in solution. The diffusion of this redox species is hindered due to a combination of steric effects (the complementary DNA hybridizing the immobilised DNA) and electrostatic effects (additional negative charges are introduced by the target DNA, which cause repulsion to the ferrocyanide/ferricyanide ions diffusing through the pores).

For the experiments, different concentrations of target DNA in 0.1 M PBS buffer, pH 7.4, starting from 0.1 pM up to 1 μM were incubated on the sensors. Three sensors and three controls were used to check the reproducibility of the sensing platform prepared with pAOO membranes.

For the electrochemical sensing experiments, first the C-SPEs were activated as described initially in 2.3.4 section of this thesis. Next, DNA-modified pAAO membranes were placed on top of these electrodes (Figure 24a) and they were clamped in an in-house custom built teflon cell with the possibility to use external reference and auxiliary electrodes (Figure 24b).

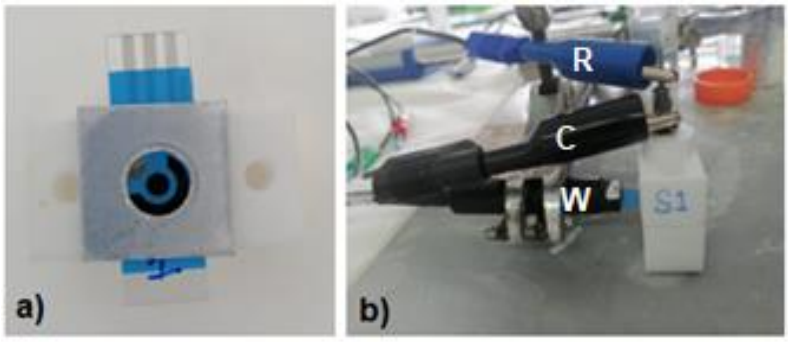

Figure 24. a) Assembly of the fabricated membranes on the C-SPE, b) cell containing the electrode and the fabricated membrane. The electrochemical cell was comprised of a working electrode (W), a reference electrode (R) and a counter electrode (C) that closes the electrical circuit.

The electrochemical response using CV, EIS and SWV was recorded for all the membrane-modified sensors in 2 mM ferrocyanide and 2 mM ferricyanide solution prepared in PBS. Measurements were repeated till stability was achieved prior to incubating the target DNA (Figure 24).

For our studies, sensing experiments were performed using sensors prepared with:

- Commercial pAAO membranes over C-SPE electrodes
- Fabricated pAAO membranes over C-SPE electrodes

3.2.1 Commercial pAAO membranes over C-SPE electrodes

Initially before proceeding with experiments using fabricated pAAO membranes, 20 nm-pore commercial pAAO membranes were used, placed on top of C-SPEs. It is important to note that these commercial membranes pose certain limitations owing to the prospects of modulating the geometric features such as pore diameter and membrane thickness as well as the homogeneity of the porous structure. These membranes were used as purchased and modified following the same protocols as the fabricated membranes.

The sensing experiments for all the sensing platforms tested was done as described in the previous section. Results using EIS and SWV as detection techniques are shown below.

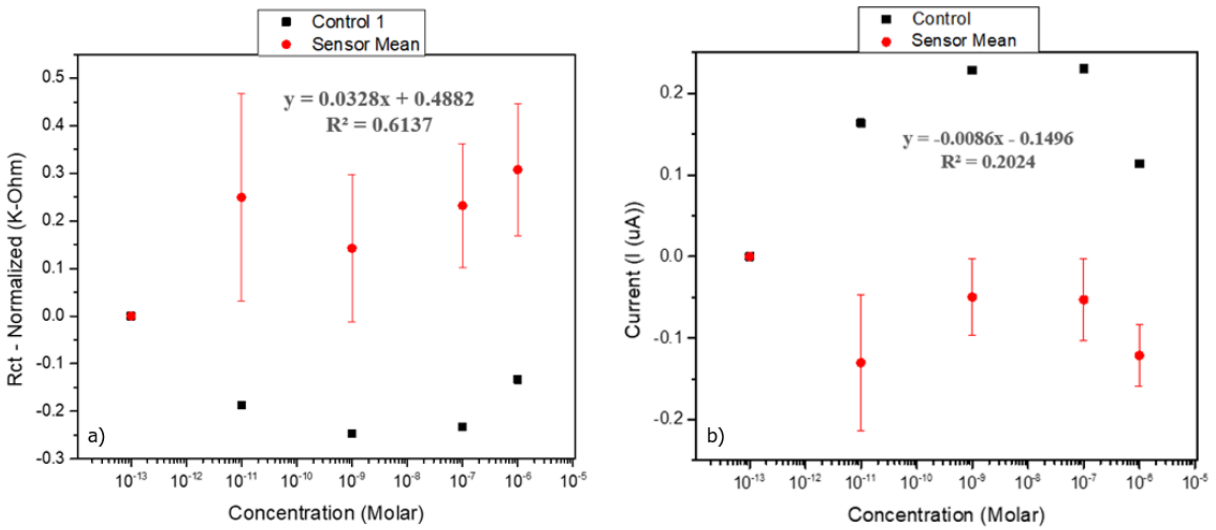

Figure 25. EIS results (a) and SWV results (b) corresponding to one control (the other two controls broke down in the functionalization process) and three sensors prepared with commercial pAAO membranes on C-SPEs.

The performance of the sensors were compared against the response from the control cells prepared with a different oligonucleotide with no affinity to the target.

EIS and SWV were used as detection techniques. Further, the EIS data were fitted into a Randle's circuit and charge transfer resistance was obtained for each sensor and control at all concentrations. Owing to increasing hindrance to the diffusion of redox species with increased concentrations of the target DNA, the charge transfer resistance is expected to increase (Figure 25a). Also, the peak current in SWV is expected to decrease whereas for controls, the charge transfer resistance and peak current values are expected to be stable as no DNA binding is expected (Figure 25b).

Even though the sensors display response different from controls, the reproducibility between the three sensors is not good which can be attributed to non homogeneous pore size distribution.

3.2.2 Fabricated pAAO membranes over C-SPE electrodes

The sensing experiment with the commercial membranes concluded that the sensors and control cell had a different response. Moreover, the response was not linear, what could be attributed to the limitations posed with using commercial membranes. Hence, pAAO membranes with homogenous pore size distribution (45 nm ± 5 nm) were fabricated with membrane thickness of almost half as those of commercial membranes (30 µm compared to 60 µm). Three sensors and controls each were used for sensing experiments.

Similar to the sensing experiments with commercial membranes, EIS and SWV were used as electrochemical detection techniques. Figure 26a and Figure 26b compare EIS and SWV results, respectively, using 3 sensors and 3 controls. As shown before, the charge transfer resistance is plotted against the concentration of target DNA sequence from EIS results whereas the peak current against the increasing concentrations of target DNA is presented for SWV.

This experiment shows much higher sensitivity (slope of the calibration curve) compared to the experiment with commercial membranes. The improved results could be attributed to the homogeneous distribution of well aligned pores in the fabricated membranes, in addition to the better control in pore size compared to commercial membranes.

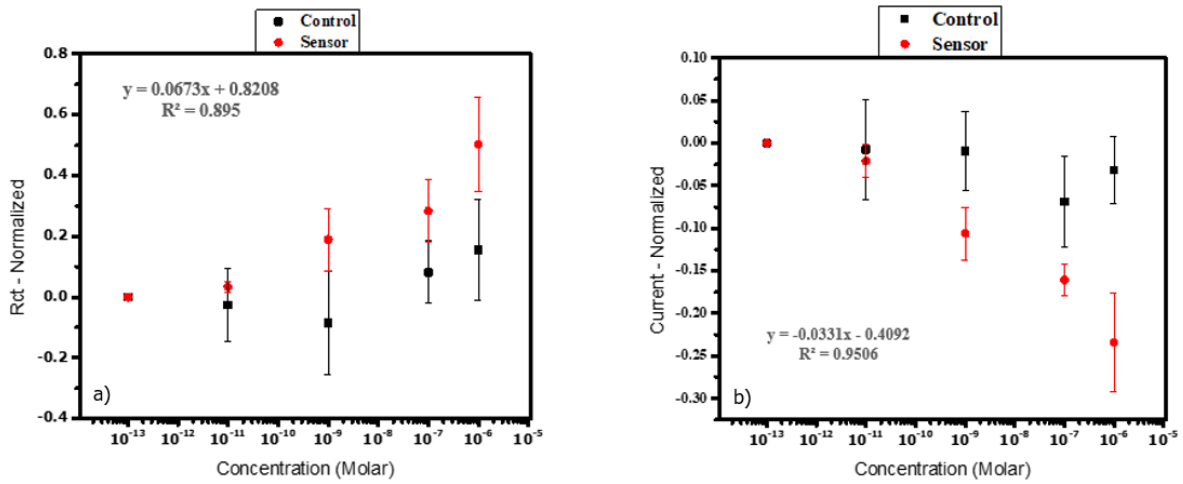

Figure 26. EIS (a) and SWV (b) results corresponding to three controls and three sensors prepared with the first set of fabricated pAAO membranes on C-SPEs.

4 Conclusions and future work

The work performed aimed at developing an electrochemical sensor with the sensitivity required to detect a specific miRNA identified as biomarker for the early stages of ALL. Initial studies were performed with a model DNA sequence as target analyte, as DNA is cheaper and more stable than RNA, so it is a good model for optimization purposes.

With the purpose of developing a highly sensitive sensor, the design of the platform was selected to allow a sensing mechanism based on pore blockage, as this has been reported to improve the sensitivity compared to sensors based on flat electrodes.

The first studies focused on comparing the response of sensors prepared with commercial pAAO membranes against those prepared with pAAO membranes fabricated in the lab. It is worth noting that sensors prepared with fabricated membranes showed a much more reproducible response and better sensitivity compared to those prepared with commercial membranes. This can be attributed to a better and more uniform pore size distribution as well as a lower thickness of these membranes. Moreover, the morphology of the fabricated membranes can be easily tuned and thus they are better suited for our studies.

Further experiments will involve a pore-size optimization study to maximize pore blockage, and thus improve sensitivity as well as blocking the top surface of the membranes for the same motivation, to restrict hybridization to occur within the pores. Next, incubation time, ssDNA capture probe concentration, etc, will be also optimized to maximize the sensitivity. Then, a selectivity study will be performed, to assess the sensor response against similar oligonucleotides, before shifting to RNA as target analyte instead of DNA. Finally, the sensors will be challenged with serum to evaluate matrix effects, and if they are significant, alternative functionalization strategies will be studied to modify the membrane surface.

The need to further develop the sensor to allow capture of exosomes and sequential detection of a target exosomal miRNA is key to exploring new ways to detect and diagnose cancer quickly, efficiently and more accurately, in this case, ALL.

5 References

[1] Mancero Rodríguez, M. J., Arellano Salinas, K. D. la P., Santo Cepeda, K. A., & Rodríguez Revelo, M. E. (2020). "Leucemia linfoblástica aguda diagnostico". RECIMUNDO, 4(2), 53-63. Available: https://doi.org/10.26820/recimundo/4.(2).mayo.2020.53-63

[2] PDQ® sobre el tratamiento pediátrico. PDQ Tratamiento de la leucemia linfoblástica aguda infantil. Bethesda, MD: National Cancer Institute. Actualización: <22/10/2021>. Disponible en: https://www.cancer.gov/espanol/tipos/leucemia/paciente/tratamiento-lla-infantil-pdq . Fecha de acceso: <19/12/2021>.

[3] Be The Match, "Trasplante y Leucemia Linfoblástica Aguda (LLA)", 2015 National Marrow Donor Program, NPO1422, MAR 2015, pag. 1-2. Available: Trasplante-y-leucemia-linfoblastica-aguda-LLA.pdf (bethematch.org.mx)

[4] Jaqueline Carvalho de Oliveira, Carlos Alberto Scrideli, María Sol Brassesco, Andressa Gois Morales, Julia Alejandra Pezuk, Rosane de Paula Queiroz, José Andres Yunes, Silvia Regina Brandalise, Luiz Gonzaga Tone, "Differential MiRNA expression in childhood acute lymphoblastic leukemia and association with clinical and biological features", Leukemia Research, Volume 36, Issue 3, 2012, Pages 293-298, ISSN 0145-2126. Available: https://doi.org/10.1016/j.leukres.2011.10.005

[5] Giovannetti, Elisa; Duyu, Muhterem; Durmaz, Burak; Gunduz, Cumhur; Vergin, Canan; Yilmaz Karapinar, Deniz; Aksoylar, Serap; Kavakli, Kaan; Cetingul, Nazan; Irken, Gulersu; Yaman, Yontem; Ozkinay, Ferda; Cogulu, Ozgur; 2014/05/14, "Prospective Evaluation of Whole Genome MicroRNA Expression Profiling in Childhood Acute Lymphoblastic Leukemia", BioMed Research International, Hindawi Publishing Corporation, 967585, 2014, ISSN: 2314-6133. Available: https://doi.org/10.1155/2014/967585

[6] A. A. Santos, "Structural Engineering of Nanoporous Anodic Alumina and Applications", Ph.D thesis, Department of Electronic, Electrical and Automatic Engineering, Rovira i Virgili University, Tarragona, Spain, 2010

[7] Abdel-Karim, R., and S. M. El-Raghy. "Fabrication of nanoporous alumina." Ch 7 (2016): 197-218.

[8] J. Chem. Educ. "A Practical Beginner's Guide to Cyclic Voltammetry". 2018, 95, 2, 197–206. Publication Date: November 3, 2017. Available: https://doi.org/10.1021/acs.jchemed.7b00361

[9] Lisdat, F., Schäfer, D. "The use of electrochemical impedance spectroscopy for biosensing." Anal Bioanal Chem 391, 1555 (2008). Available: https://doi.org/10.1007/s00216-008-1970-7

[10] F.R. Simões, M.G. Xavier, 6 – "Electrochemical Sensors", Editor(s): Alessandra L. Da Róz, Marystela Ferreira, Fábio de Lima Leite, Osvaldo N. Oliveira, In Micro and Nano Technologies, Nanoscience and its Applications, William Andrew Publishing, 2017, Pages 155-178, ISBN 9780323497800. Available: https://doi.org/10.1016/B978-0-323-49780-0.00006-5

[11] Patricia Batista Deroco, Juliana de Fátima Giarola, Dagwin Wachholz Júnior, Gustavo Arantes Lorga, Lauro Tatsuo Kubota, Chapter Four – "Paper-based electrochemical sensing devices", Editor(s): Arben Merkoçi, Comprehensive Analytical Chemistry, Elsevier, Volume 89, 2020, Pages 91-137, ISSN 0166-526X, ISBN 9780444643452. Available: https://doi.org/10.1016/bs.coac.2019.11.001

[12] R.K. Franklin, S.M. Martin, T.D. Strong, R.B. Brown, "Chemical and Biological Systems: Chemical Sensing Systems for Liquids", Reference Module in Materials Science and Materials Engineering, Elsevier, 2016, ISBN 9780128035818. Available: https://doi.org/10.1016/B978-0-12-803581-8.00549-X

[13] P. WESTBROEK, 2 – "Electrochemical methods", Editor(s): P. Westbroek, G. Priniotakis, P. Kiekens, In Woodhead Publishing Series in Textiles, Analytical Electrochemistry in Textiles, Woodhead Publishing, 2005, Pages 37-69, ISBN 9781855739192. Available: https://doi.org/10.1533/9781845690878.1.37

[14] M. Mazloum-Ardakani, B. Barazesh, A distinguished cancer-screening package containing a DNA sensor and an aptasensor for early and certain detection of acute lymphoblastic leukemia, Clin. Chim. Acta 497 (2019) 41–47, https://doi. org/10.1016/j.cca.2019.07.009.

[15] Zixue S.," Porous anodic metal oxides ", University of St. Andrews, Scotland, 2009.

[16] BOOK. Tripathi, Sadhna. Sumi, Akhato. Ganguly, Sauradipta. 2018/10/25. "Performace amelioration of imported timber with environ-safe preservative ziboc". Image available online: https://www.researchgate.net/figure/JASCO-IRT-5000-infra-red-microscope-and-JASCO-FT-IR-6300-spectrometer-University-of_fig27_339069575